PHYSICAL REVIEW C VOLUME 23, NUMBER 2 FEBRUARY 1981

Self-energy in a semirealistic model of nuclear matter

V. Bernard and C. Mahaux
Institut de Physique, Université de Liège, B4000 Liège 1, Belgium
(Received 21 July 1980; revised manuscript received 22 September 1980)

A semirealistic parametrization in momentum space is used for the matrix elements of the effective nucleon-nucleon interaction. In this model, the nucleons only interact in a relative s-wave state and essentially via an exponential potential. In the Hartree-Fock approximation, algebraic expressions are derived for the self-energy and the effective mass. The strength and the range of the nucleon-nucleon interaction are chosen in such a way that these quantities are in fair agreement with the empirical values. We calculate analytically the frequency dependence of the imaginary part of the polarization and correlation contributions to the self-energy. The real part of these contributions can then be computed very accurately with the help of dispersion relations. Their frequency dependence can most conveniently be described in terms of a frequency mass $\bar{m}$. It is found that $\bar{m}$ has an enhancement peak, typically 30 MeV wide, centered on the Fermi energy. The contributions of the correlation and of the polarization graphs to this local enhancement are disentangled. The contribution to $\bar{m}$ of the polarization graph peaks somewhat above the Fermi energy, and that of the correlation graph somewhat below the Fermi energy. The total peak is approximately symmetric about the Fermi energy. We identify the range of excitation energy of those core excited states which mainly contribute to the enhancement. The enhancement peak is more pronounced at low density and for long-range interactions. The usual effective mass also displays an enhancement at the Fermi surface. The momentum distribution in the correlated ground state is calculated. The effect of introducing a hard core in the nucleon-nucleon interaction is studied.

[NUCLEAR STRUCTURE Second order approximation to self-energy of nucleons in nuclear matter.]

I. INTRODUCTION

In the independent-particle model, the nucleons are assumed to move independently of one another in an average potential field. In the Hartree-Fock approximation, this average field is nonlocal and independent of the frequency of the nucleon. Higher order corrections to the Hartree-Fock approximation introduce a frequency dependence into the average field. Much interest has recently been devoted to this frequency dependence,[1-6] to which the present paper is mainly devoted. Empirical hints to the existence of a striking and sizable frequency dependence had first been pointed out by Brown, Gunn, and Gould.[7] These authors exhibited the following problem. The Hartree-Fock approximation to the average single-particle field yields a strongly nonlocal single-particle potential which accounts well for the properties of the scattering and of the deeply bound single-particle states, but fails to yield the density of single-particle levels near the Fermi surface. Indeed, the latter can be reproduced with a purely *local* field. The existence of this problem has since been repeatedly confirmed.[8] Bertsch and Kuo[9] showed that it is likely to be qualitatively solved if one takes into account the fact that single-particle states are shifted due to their coupling to low-lying core excited states. This coupling gives rise to a frequency dependence of the average nuclear field. The effect of this frequency dependence appears to approximately cancel that of the nonlocality near the Fermi surface, and is believed to disappear far from the Fermi surface. In the work of Bertsch and Kuo, the core excited states were taken as mixed particle-hole excitations. They were described as vibrational phenons by Hamamoto and Siemens[10] and as random-phase approximation excitations by Bernard and Van Giai.[6] While these more recent works confirm that single-particle energies are compressed in the vicinity of the Fermi surface, they are unable to give a measure of the size of the energy domain in which this compression takes place. It has recently been shown that this size plays an important role.[2,3] An estimate is given in Refs. 2 and 9. It is very hard to perform it in a reliable way, partly because of the limited configuration space which can in practice be included, and partly because of the difficulty of uniquely identifying a quasiparticle state in a calculation which yields fragmented single-particle states. It is thus of interest to study infinite nuclear matter, where the quasiparticle states can be unambiguously defined, and where, furthermore, all relevant quantities can be plotted as smooth functions of the quasiparticle frequency or momentum. Our results also provide an instructive and explicit illustration in the case of nuclear matter of the arguments which have been used in Ref. 2 to estimate the size of the energy domain in which the compression of the single-particle level den-

sity takes place.

When the standard Brueckner-Hartree-Fock approximation is modified so as to include *low-lying* one-particle–one-hole excitations, a striking frequency dependence of the single-particle field is found,[11] which appears to semiquantitatively account for the compression of single-particle energies near the Fermi surface.[4,5,12] The Brueckner-Hartree-Fock approximation presents the benefit of enabling one to use realistic nucleon-nucleon interactions. In the present context, however, it suffers from the following drawbacks. Firstly, it only sums particle-particle ladders, and therefore does not include the so-called correlation (or Pauli rearrangement) term. This is a severe disadvantage since this correlation term is shown below to play a very significant role in the frequency dependence of the field near the Fermi surface. Secondly, it is very hard to carry out a Brueckner-Hartree-Fock calculation with a numerical accuracy sufficient to investigate in detail phenomena which are localized in a narrow frequency domain. Thirdly, the physical origin of the numerical results is rather difficult to ascertain because of the complexity of the calculation. This prompted the present work in which we use a simple analytical model originally due to Brueckner.[13]

In Sec. II, we briefly recall a few basic definitions and properties. The analytical model[13] is introduced and discussed in Sec. III; it is closely related to an exponential effective nucleon-nucleon interaction which acts only in relative s-wave states. In Sec. IV, we derive analytic expressions for the first order (Hartree-Fock) approximation to the single-particle field and to the effective mass. We establish contact with the Landau theory of Fermi liquids. We also discuss the choice of the input parameters contained in the model. Sec. V is devoted to the polarization contribution to the average field, which arises from the fact that the addition of a nucleon to the ground state of nuclear matter gives rise to core excited states. We calculate analytically the frequency dependence of the imaginary part of the polarization graph. The real part of this contribution is then computed from a dispersion relation. The accuracy is extremely good, and we can thus show in full detail that the frequency dependence of the real part is enhanced in the vicinity of the Fermi surface. We analyze how this enhancement depends upon the nuclear matter density and upon the range of the effective nucleon-nucleon interaction. The effect of a hard core is investigated. We also identify the energy of those core excited states which mainly contribute to the enhancement. In Sec. VI, we investigate the correlation graph, which accounts for the fact that in the presence of an additional nucleon some virtual excitations of the correlated ground state of nuclear matter are forbidden by the Pauli principle. This graph had never been accurately computed previously, except in the somewhat academic case of the dilute hard sphere Fermi gas model.[12] The other previous evaluations[14-18] were too inaccurate to yield the frequency dependence of this graph. We use here a dispersion relation approach as in the case of the polarization contribution. The frequency dependence of the polarization and of the correlation graphs is intimately related to the momentum distribution of the nucleons in the correlated ground state, which we thus also calculate. Section VII is devoted to the effective mass which determines the density of the single-particle states. The sum of the Hartree-Fock, of the polarization, and of the correlation graphs yields an effective mass which is state dependent and displays a narrow enhancement at the Fermi surface. Section VIII contains a brief summary and our main results.

II. DEFINITIONS AND PROPERTIES

The single-particle field can be identified with the self-energy (or mass operator).[11] This is a nonlocal, complex, and frequency-dependent operator that we denote by $\mathcal{U}(\vec{r},\vec{r}';\omega)+i\mathcal{W}(\vec{r},\vec{r}';\omega)$. In infinite nuclear matter, it only depends on the frequency ω and on $|\vec{r}-\vec{r}'|$. A Fourier transformation over the latter variable yields the momentum and frequency dependent mean field

$$\Sigma(k;\omega)=V(k;\omega)+iW(k;\omega)\,. \tag{2.1}$$

The first three terms of the expansion of $\Sigma(k;\omega)$ in powers of the strength of the nucleon-nucleon interaction are represented in Fig. 1. The first

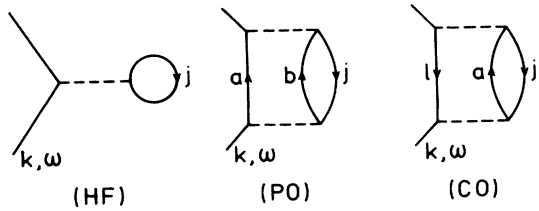

FIG. 1. Graphical representation of the first three terms of the perturbation expansion of the single-particle field. The exchange terms are not drawn, for simplicity. A horizontal dashed line is associated with the nucleon-nucleon interaction. An upward pointing arrow corresponds to a particle intermediate state and a downward pointing arrow corresponds to a hole intermediate state. The graph labeled HF shows the Hartree-Fock approximation, while graphs PO and CO represent the second-order polarization and correlation contributions, respectively.

order contribution is labeled (HF) and corresponds to the Hartree-Fock approximation. It is independent of frequency and its algebraic expression reads

$$\Sigma_{HF}(k;\omega)=V_{HF}(k)=\sum_{\vec{j}} n_<(j)\langle \vec{k},\vec{j}\,|v|\,\vec{k},\vec{j}-\vec{j},\vec{k}\rangle . \quad (2.2)$$

Here

$$n_<(j)=1-n_>(j)=\theta(k_F-j), \quad (2.3)$$

where k_F denotes the Fermi momentum and v the nucleon-nucleon interaction. We dropped explicit reference to the spin and isospin degrees of freedom. The second order contribution labeled (PO) is the polarization graph. Its algebraic expression reads

$$\Sigma_{PO}(k;\omega)=\tfrac{1}{2}\sum_{\vec{a},\vec{b},\vec{j}} n_>(a)n_>(b)n_<(j)\times\frac{|\langle \vec{a},\vec{b}|v|\,\vec{k},\vec{j}-\vec{j},\vec{k}\rangle|^2}{\omega+e(j)-e(a)-e(b)-i\eta}, \quad (2.4)$$

where $e(j)$ is defined by the energy-momentum relation ($\hbar=1$)

$$e(j)=\frac{j^2}{2m}+V_{HF}(j), \quad (2.5)$$

where m is the nucleon mass. Graph (CO) in Fig. 1 represents the second order correlation contribution. One has

$$\Sigma_{CO}(k;\omega)=\tfrac{1}{2}\sum_{\vec{j},\vec{l},\vec{a}} n_<(j)n_<(l)n_>(a)\times\frac{|\langle \vec{j},\vec{l}|v|\,\vec{k},\vec{a}-\vec{a},\vec{k}\rangle|^2}{\omega+e(a)-e(j)-e(l)-i\eta}. \quad (2.6)$$

If $W_{PO}(k;\omega)$ and $W_{CO}(k;\omega)$ approach zero as $|\omega|$ tends towards infinity, a dispersion relation holds, which will be used in the following:

$$V_{PO}(k;\omega)=\frac{P}{\pi}\int_{\omega_F}^{\infty}\frac{W_{PO}(k;\omega')}{\omega-\omega'}d\omega' . \quad (2.7)$$

$$V_{CO}(k;\omega)=\frac{P}{\pi}\int_{-\infty}^{\omega_F}\frac{W_{CO}(k;\omega')}{\omega-\omega'}d\omega' . \quad (2.8)$$

Here P refers to a principal value integral, while $\omega_F=e(k_F)$ is the Hartree-Fock approximation to the Fermi energy.

III. THE MODEL

The dependence upon relative momentum of the diagonal elements of the Brueckner reaction matrix between two plane waves can be reproduced fairly well by an effective potential which has finite range and only acts in low, even relative partial waves.[19,20] In order to minimize the number of parameters, we adopt here a spin- and isospin-independent exponential potential

$$v(r)=v_0\exp(-\mu r) \quad (3.1)$$

and we let it act only in the s-partial wave. The matrix elements of v between plane wave states can be calculated in a straightforward manner. One finds

$$\langle \vec{k},\vec{j}\,|v|\,\vec{a},\vec{b}\rangle=\frac{8\pi\mu v_0}{[\mu^2+(\tfrac{1}{2}|\vec{k}-\vec{j}|)^2+(\tfrac{1}{2}|\vec{a}-\vec{b}|)^2]^2-(\tfrac{1}{2}|\vec{a}-\vec{b}||\vec{k}-\vec{j}|)^2} . \quad (3.2)$$

In order to further simplify the model, and to retrieve a model previously considered in Refs. 11 and 13, we drop the last term in the denominator on the right-hand side of Eq. (3.2). The model s-wave interaction used in the present paper is thus defined by the following equation:

$$\langle \vec{k},\vec{j}\,|v|\,\vec{a},\vec{b}\rangle=\frac{8\pi\mu v_0}{(\mu^2+\frac{1}{4}|\vec{k}-\vec{j}|^2+\frac{1}{4}|\vec{a}-\vec{b}|^2)^2} . \quad (3.3)$$

IV. HARTREE-FOCK APPROXIMATION

The model interaction (3.3) contains two parameters, namely the potential strength v_0 and the potential range μ^{-1}. Note that μ has the meaning of a range in momentum space. In the present context, one sensible way of determining typical values for these parameters appears to consist in requiring that the Hartree-Fock approximation be in fair agreement with empirical evidence concerning the single-particle field. The Hartree-Fock approximation to the single-particle field in the present model can be calculated analytically. We find

$$V_{HF}(k)=\frac{6\sqrt{2}v_0}{\pi}\left[\tan^{-1}\left(\frac{k+k_F}{\mu\sqrt{2}}\right)-\tan^{-1}\left(\frac{k-k_F}{\mu\sqrt{2}}\right)-\frac{1}{\sqrt{2}}\ln\frac{(k+k_F)^2+2\mu^2}{(k-k_F)^2+2\mu^2}\right] . \quad (4.1)$$

Empirically, it is known that the depth of the single-particle field at the nuclear center and at low energy is equal to approximately -54 MeV.[21] This may be used to fix the value of the potential strength for a given range μ^{-1}. It is convenient to characterize the potential strength by the ratio v_0/μ^3, to which the volume integral of the exponential interaction (3.1) is proportional. In Fig. 2, we plot the Hartree-Fock potential $V_{HF}(k)$ for the Fermi momentum $k_F=1.35$ fm^{-1} and for the following two sets of parameter values

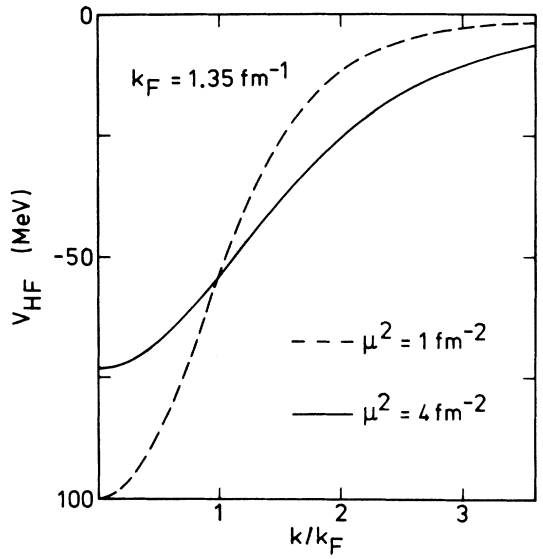

FIG. 2. Dependence upon k/k_F of the Hartree-Fock approximation to the single-particle field for $k_F = 1.35$ fm^{-1} and for the parameter sets (4.2a) (full curve) and (4.2b) (dashed curve).

$$v_0/\mu^3 = 30\ \text{MeV fm}^3,\ \mu^2 = 4\ \text{fm}^{-2}, \tag{4.2a}$$

$$v_0/\mu^3 = 70.6\ \text{MeV fm}^3,\ \mu^2 = 1\ \text{fm}^{-2}. \tag{4.2b}$$

These two sets yield the same potential depth at the Fermi surface, namely $V_{HF}(k_F) = -54.2$ MeV for $k_F = 1.35$ fm^{-1}. We now argue that the corresponding values of μ^2 encompass the plausible range of values. One must be somewhat careful when interpreting μ^{-1} as the range of the effective nucleon-nucleon interaction, since the "range" depends on the radial dependence of $v(r)$. Many empirical analyses assume that $v(r)$ has a Yukawa shape[22] $v_Y(r) = v_Y{}^0 \exp(-\beta r)/\beta r$. In order to compare the "ranges" of different interactions, it is useful to consider their mean square radius $\langle r^2 \rangle$. In the case of the exponential form factor (3.1) one has $\langle r_Y{}^2 \rangle = 12\,\mu^{-2}$, while the Yukawa shape yields $\langle r_Y{}^2 \rangle = 6\beta^{-2}$. For the exponential potential (3.1), one has $\langle r_v{}^2 \rangle = 12$ fm^2 for $\mu^2 = 1$ fm^{-2}, and $\langle r_v{}^2 \rangle = 3$ fm^2 for $\mu^2 = 4$ fm^{-2}. This should be compared with $\langle r_Y{}^2 \rangle \approx 12.7$ fm^2 in the case of a Yukawa potential associated with one-pion exchange, and $\langle r_Y{}^2 \rangle \approx 3.2$ fm^2 in the case of two-pion exchange.

Figure 2 shows that the Hartree-Fock fields which correspond to the two parameter sets (4.2a) and (4.2b) have a quite different momentum dependence. The latter can be characterized by the following quantity that was called "k mass" in Ref. 11 and that we henceforth call the "momentum mass":

$$\tilde{m}(k) = m\left[1 + \frac{m}{k}\frac{d}{dk} V_{HF}(k)\right]^{-1}. \tag{4.3}$$

The usual "effective mass" m^* reduces to $\tilde{m}$ in the Hartree-Fock approximation. Figure 3 shows that $\tilde{m}(k)$ is a rather smooth function of k in the domain $1.5\ k_F > k > 0.5\ k_F$ in which we shall mainly be interested. Unless otherwise specified, all values of $\tilde{m}$ quoted below are evaluated at the Fermi surface, i.e., $\tilde{m} = \tilde{m}(k_F)$. The fact that $\tilde{m}$ differs from m corresponds to the property that the Fourier transform $v_{HF}(|\vec{r} - \vec{r}'|)$ of $V_{HF}(k)$ is a non-local potential.

The effective mass is one of the fundamental parameters of Landau's theory of Fermi liquids. There, the particle hole interaction $w(\vec{k}, \vec{j})$ for $k = j = k_F$ is expanded in multipoles

$$w(\vec{k}, \vec{j}) = \sum_L f_L P_L(\cos\phi), \tag{4.4a}$$

where ϕ is the angle between $\vec{k}$ and $\vec{j}$. From Galilean invariance, one derives the relation $m^*/m = 1 + \frac{1}{3}F_1$ between the effective mass m^* measured at the Fermi surface and the Landau parameter $F_1 = 2\pi^{-2} m^* k_F f_1$. In the framework of the Hartree-Fock approximation, one has[23]

$$w(\vec{k}, \vec{j}) = \langle \vec{k}, \vec{j} | v | \vec{k}, \vec{j} \rangle - \langle \vec{k}, \vec{j} | v | \vec{j}, \vec{k} \rangle. \tag{4.4b}$$

A straightforward calculation yields

$$f_1 = 9\pi \frac{v_0}{\mu^3} \alpha^{-4}\left[\frac{2\alpha^2(1+\alpha^2)}{1+2\alpha^2} - \ln(1+2\alpha^2)\right], \tag{4.5}$$

where $\alpha = k_F/\mu$. It can be checked that the expression of $\tilde{m}$ calculated from Eq. (4.5) is identical to the one which is obtained from Eqs. (4.1) and (4.3).

V. CONTRIBUTION OF THE POLARIZATION GRAPH

A. Introduction

The second-order polarization contribution to the single-particle field is represented by the graph labeled (PO) in Fig. 1. Its physical inter-

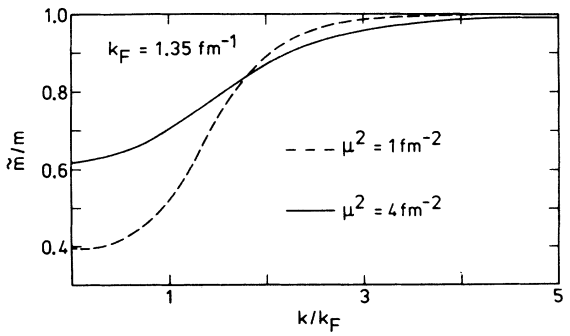

FIG. 3. Dependence upon k/k_F of the momentum mass $\tilde{m}$ measured in units of the bare mass m for $k_F = 1.35$ fm^{-1} and for the parameter sets (4.2a) (full curve) and (4.2b) (dashed curve).

pretation is the following [see Eq. (2.4)]. When a nucleon with momentum $\vec{k}$ and frequency ω is added to the ground state of nuclear matter, it can interact with a nucleon with momentum $\vec{j}$. As a result, a two-particle–one-hole intermediate state is formed. This intermediate state is a real excitation if energy is conserved, i.e., if $\omega = e(a) + e(b) - e(j)$; otherwise it is a virtual excitation. The real excitations give rise to an imaginary component of the mean field, namely

$$W_{\mathrm{PO}}(k;\omega) = \frac{\pi}{2} \sum_{\vec{a},\vec{b},\vec{j}} n_>(a) n_>(b) n_<(j) \times |\langle \vec{a},\vec{b}|v|\vec{k},\vec{j}-\vec{j},\vec{k}\rangle|^2 \times \delta(\omega + e(j) - e(a) - e(b)) . \quad (5.1)$$

The real part of the polarization graph reads

$$V_{\mathrm{PO}}(k;\omega) = \tfrac{1}{2} \sum_{\vec{a},\vec{b},\vec{j}} n_>(a) n_>(b) n_<(j) \frac{|\langle \vec{a},\vec{b}|v|\vec{k},\vec{j}-\vec{j},\vec{k}\rangle|^2}{\omega + e(j) - e(a) - e(b)} , \quad (5.2)$$

where the summation sign implies a principal value integral whenever the energy denominator on the right-hand side vanishes. Momentum conservation requires that

$$\vec{k} + \vec{j} = \vec{a} + \vec{b} (= 2\vec{p}) . \quad (5.3)$$

Here, we shall mainly be interested in the dependence upon ω of the derivatives $\partial V_{\mathrm{PO}}(k;\omega)/\partial\omega$ and $\partial V_{\mathrm{CO}}(k;\omega)/\partial\omega$. These quantities strongly depend upon ω in the vicinity of the Fermi energy ω_F. The detailed investigation of this phenomenon implies the calculation of second derivatives with respect to ω of $V_{\mathrm{PO}}(k;\omega)$ and $V_{\mathrm{CO}}(k;\omega)$. Even the recourse to Monte Carlo integration techniques[17,18] does not yield sufficient accuracy for this purpose, whence the interest in considering simplified models in which most of the calculation can be performed analytically. To our knowledge, only two such models have been considered in the past. The first one is the dilute hard sphere Fermi gas model.[12] The other model is the one which is studied here. It had been introduced by Brueckner,[13] who evaluated the derivative $\partial V_{\mathrm{PO}}(k;\omega)/\partial\omega$ at $\omega = e(k)$. Brueckner's study was restricted to the domain $k < k_F$ in which the denominator on the right-hand side of Eq. (5.2) does not vanish. Jeukenne *et al.*[11] have extended Brueckner's work to the domain $k > k_F$, in which difficulties arise since there one is not allowed to commute the summation sign in Eq. (5.2) with a derivative with respect to ω. In Refs. 11 and 13 a perturbation expansion in powers of $(k - k_F)^2/\mu^2$ was used, as well as several approximations (e.g., $p \approx k_F$) which we have found to be quite inaccurate. Furthermore, these authors had not been able to apply their perturbation technique to the correlation graph. This is a serious limitation since the correlation graph is as important as the polarization graph near the Fermi surface. For these reasons, and also because this will lead to a better physical interpretation of our results, we shall in the present paper use the same approach as the one which was adopted in Ref. 12 in the case of the dilute hard sphere Fermi gas. We shall thus first derive an analytic expression for the imaginary part of the polarization graph and then calculate the real part and its derivative from the dispersion relation (2.7). The same approach will be used for the correlation graph in Sec. VI.

B. Imaginary part of the polarization graph

The main reason why the imaginary part of the polarization graph is easier to evaluate than its real part is that the δ function on the right-hand side of Eq. (5.1) reduces the problem to the calculation of a three-dimensional integral; the integrand, moreover, has a simpler form in Eq. (5.1) than in Eq. (5.2). In the case of the dilute hard sphere Fermi gas, straightforward but very lengthy calculations lead to algebraic expressions for $W_{\mathrm{PO}}^{\mathrm{HS}}(k;\omega)$ in the whole $(k;\omega)$ plane.[12] We believe that this could also be achieved in the present model. In view of the forbidding character of these calculations we shall, however, limit ourselves here to the calculation of the second order graphs at $k = k_F$. This is justified by the fact that we are mainly interested in the domain $1.5\ k_F > k > 0.5\ k_F$ in which the dependence of $W_{\mathrm{PO}}(k;\omega)$ and $W_{\mathrm{CO}}(k;\omega)$ upon k is much weaker than their dependence upon ω.[11,12] Accordingly, we henceforth usually drop explicit reference to the argument k_F and write, for instance, $W_{\mathrm{PO}}(k_F;\omega) = W_{\mathrm{PO}}(\omega)$. The results presented below are thus exact at $k = k_F$ but may be inaccurate by typically twenty percent for $|k - k_F| \approx 0.5\ k_F$. This inaccuracy is quite tolerable in view of the semirealistic character of the model.

If one limits oneself to second order in the strength of the nucleon-nucleon interaction one may replace the energy $e(q)$ by $q^2/2m$ in the denominator on the right-hand side of Eqs. (2.4) and (2.6). A better approximation consists in taking $e(q) = q^2/2\tilde{m}$, where $\tilde{m}$ is the momentum mass discussed in Sec. IV. Equation (5.1) then becomes

$$W_{\mathrm{PO}}(\omega) = \pi\tilde{m} \sum_{\vec{a},\vec{b},\vec{j}} n_>(a) n_>(b) n_<(j) \times |\langle \vec{a},\vec{b}|v|\vec{k},\vec{j}-\vec{j},\vec{k}\rangle|^2 \times \delta(2\tilde{m}\omega + j^2 - a^2 - b^2) . \quad (5.4)$$

Quite lengthy calculations lead to unwieldy alge-

braic expression of the right-hand side of Eq. (5.4). These can be provided upon request. These algebraic results enable us to compute $W_{PO}(\omega)$ and all related quantities with very good accuracy. The dependence of W_{PO} upon $\omega-\omega_F$ is shown in Fig. 4. The fact that $W_{PO}(\omega)$ vanishes at $\omega=\omega_F$ directly reflects the decrease of the density of two-particle–one-hole states at the Fermi surface. For ω close to ω_F, one has indeed

$$W_{PO}(\omega)\approx\frac{\pi}{(2\pi)^4}(m\tilde{})^3(\omega-\omega_F)^2\overline{|v|^2}\ , \tag{5.5}$$

where $\overline{|v|^2}$ denotes an average value of $|\langle\vec{a},\vec{b}|\times v|\vec{k}_F,\vec{j}-\vec{j},\vec{k}_F\rangle|^2$. Note that $\overline{|v|^2}$ slightly depends upon k_F. For large values of ω, $W_{PO}(\omega)$ decreases with increasing ω and becomes approximately proportional to the density ρ. This can be understood on the basis of the impulse approximation. In the present model, one can check that for large ω one has

$$W_{PO}(k_F;\omega)\sim\frac{8m\tilde{}}{\pi}\left(\frac{v_0}{\mu^3}\right)^2\mu^8k_F{}^3(m\tilde{}\omega)^{-7/2}\ . \tag{5.6}$$

The asymptotic laws (5.5) and (5.6) imply that, with increasing ω, $W_{PO}(\omega)$ first increases, reaches a maximum, and then decreases. This behavior is quite general; it is independent of the input parameters. The high-energy behavior (5.6) ensures that the dispersion relation (5.7) can be used as it stands in the case of the present model. This is to be contrasted with the hard sphere Fermi gas model, where one has for large ω[12]

$$W_{PO}^{HS}(k;\omega)\sim\frac{2}{\pi}k_F(k_Fc)^2\left(\frac{\omega}{m\tilde{}}\right)^{1/2}\ . \tag{5.7}$$

In that case, one must thus use a subtracted form of the dispersion relation (2.7), namely

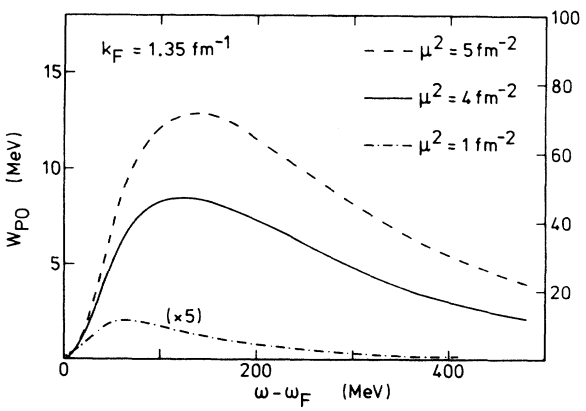

FIG. 4. Dependence upon the difference $\omega-\omega_F$ of the imaginary part of the polarization graph, for k_F=1.35 fm^{-1}, and for μ^2=1 fm^{-2} (dash-and-dot curve), μ^2=4 fm^{-2} (full curve), or μ^2= 5 fm^{-2} (dashes). Here, v_0/μ^3 = 30 MeV fm^3.

$$V_{PO}(k;\omega)=V_{PO}(k;\omega_0)+(\omega_0-\omega)\frac{1}{\pi}\times\int_{\omega_F}^{\infty}\frac{W_{PO}(k;\omega')}{(\omega_0-\omega')(\omega-\omega')}d\omega'\ , \tag{5.8}$$

where ω_0 is arbitrary

C. Real part of the polarization graph

Since $W_{PO}(k_F;\omega)$ is known, we can calculate the real part $V_{PO}(k_F;\omega)$ of the polarization graph from the dispersion relation (2.7) or, equivalently, from the subtracted dispersion relation (5.8). If we take $\omega_0=\omega_F$, the latter reads

$$V_{PO}(k;\omega)-V_{PO}(k;\omega_F)=\pi^{-1}(\omega-\omega_F)\int_0^{\infty}\frac{W_{PO}(k;\omega_F+z)}{z[z-(\omega-\omega_F)]}dz\ . \tag{5.9}$$

This relation and the asymptotic behavior (5.5) show that at $\omega=\omega_F$ the real part $V(k;\omega)$ has a logarithmic singularity of the type[24]

$$(\omega-\omega_F)^2\ln(\omega-\omega_F)\ . \tag{5.10}$$

This singularity is quite weak. It implies, however, that the second derivative $(\partial/\partial\omega)[\partial V_{PO}\times(k_F;\omega)/\partial\omega]$ is infinite at $\omega=\omega_F$. The numerical investigation of this property requires a very accurate calculation of $V_{PO}(k;\omega)$. This is feasible here since we know $W_{PO}(\omega)$ in analytical form, and since Eq. (2.7) can then be used to obtain $V_{PO}(\omega)$ with arbitrary accuracy. This is the main advantage of the present model and approach.

The quantity $V_{PO}(\omega)$ is represented in the lower part of Fig. 5. Its main features can be understood from the dispersion relation (2.7). For ω smaller than ω_F, and by continuity also at least for ω somewhat larger than ω_F, Eq. (2.7) implies that $V_{PO}(\omega)$ is negative. This is also clear from Eq. (5.2). For $\omega<\omega_F$, one can write

$$\frac{\partial}{\partial\omega}V_{PO}(\omega)=-\frac{P}{\pi}\int_{\omega_F}^{\infty}\frac{W_{PO}(\omega')}{\omega-\omega'}d\omega'\ , \tag{5.11}$$

so that $V_{PO}(\omega)$ is then a decreasing function of ω. The relation (5.11) does not hold for $\omega>\omega_F$. Indeed, the integral sign in Eq. (2.7) may in general not be commuted with the operator $\partial/\partial\omega$ when the integrand is singular. As a matter of fact, the shape of $W_{PO}(\omega)$ implies that $V_{PO}(\omega)$ must change sign in the domain $\omega>\omega_F$. Its derivative must thus be negative at $\omega\approx\omega_F$ and positive at large ω.

We now discuss the dependence of the polarization graph upon the parameter μ. As noted before, the latter has the physical meaning of a potential range in momentum space. Figure 4 shows that for a given value of v_0/μ^3, the imaginary part $W_{PO}(\omega)$ strongly decreases with decreasing μ^2,

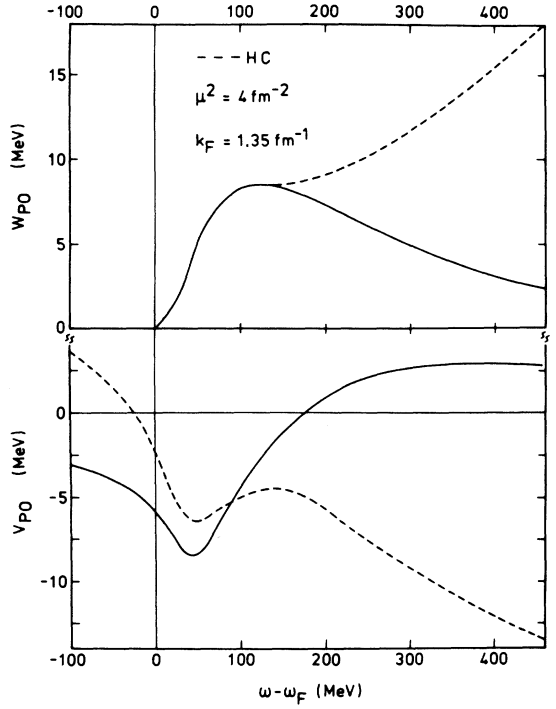

FIG. 5. The full curves represent the dependence upon $\omega - \omega_F$ of the quantities $W_{PO}(\omega)$ (upper part) and $V_{PO}(\omega)$ (lower part) for $\mu^2 = 4$ fm^{-2}, $k_F = 1.35$ fm^{-1}, and $v_0/\mu^3 = 30$ MeV fm^3. The dashes correspond to a modification of the model as described by Eq. (5.28), in order to simulate the effect of a hard core repulsion.

except for very small values of $\omega - \omega_F$. The dispersion relation (2.7) then implies that $|V_{PO}(\omega)|$ decreases when μ^2 decreases. The origin of the decrease of $W_{PO}(\omega)$ with decreasing μ^2 is the following. The density of two-particle–one-hole states is independent of μ. When μ^2 is small, the strength with which the channels labeled by the momenta $(\vec{a}, \vec{b}, \vec{j})$ are coupled to the single-particle states $(\vec{k}, \omega)$ strongly decreases with increasing $|\vec{a} - \vec{b}|$ or $|\vec{k} - \vec{j}|$. Then the effective interaction provides only inefficient coupling to all channels except those which correspond to low-lying excitations, for which $|\vec{a} - \vec{b}|$ and $|\vec{k} - \vec{j}|$ are smaller than μ. The latter remark also explains why the location of the maximum of $W_{PO}(\omega)$ drifts towards smaller values of $\omega - \omega_F$ when μ^2 decreases. We finally turn to the dependence of $W_{PO}(\omega)$ upon the Fermi momentum. For ω close to ω_F, the asymptotic behavior (5.5) indicates that $W_{PO}(\omega)$ does not depend much upon k_F. For large $\omega - \omega_F$, the impulse approximation shows that $W_{PO}(\omega)$ is proportional to k_F^3. These arguments indicate that the location of the maximum of $W_{PO}(\omega)$ drifts towards smaller values of $\omega - \omega_F$ when k_F decreases. This has been checked numerically.

D. Effective mass and related quantities

The energy ω_k of a quasiparticle with momentum k is determined by the energy-momentum relation

$$\omega_k = \frac{k^2}{2m} + V(k; \omega_k). \tag{5.12}$$

In the Hartree-Fock approximation one has $\omega_k \approx e(k)$. The dependence of the potential energy $V(\omega_k) = V(k; \omega_k)$ upon the quasiparticle energy is characterized by the effective mass m^*, with

$$\frac{m^*}{m} = 1 - \frac{d}{d\omega_k} V(\omega_k). \tag{5.13}$$

The effective mass can be written as a product of a quantity $\tilde{m}/m$ which characterizes the dependence of $V(k; \omega)$ upon the momentum k by a frequency mass $\bar{m}$ which characterizes the dependence of $V(k; \omega)$ upon the frequency ω:

$$\frac{m^*}{m} = \frac{\tilde{m}}{m} \cdot \frac{\bar{m}}{m}, \tag{5.14}$$

$$\frac{\tilde{m}}{m} = \left\{ 1 + \frac{m}{k} \left[\frac{\partial}{\partial k} V(k; \omega) \right]_{\omega = \omega_k} \right\}^{-1}, \tag{5.15}$$

$$\frac{\bar{m}}{m} = 1 - \left[\frac{\partial}{\partial \omega} V(k; \omega) \right]_{\omega = \omega_k}. \tag{5.16}$$

The quantity $Z_k = m/\bar{m}$ measures the overlap between a true single-particle state and its quasiparticle approximation. It is called the spectroscopic factor,[25] the reduced amplitude,[22] or the quasiparticle pole strength.[26] The effective mass is directly related to the density of single-particle states, since the number of proton (or neutron) single-particle states per unit energy and per unit volume is given by km^*/π^2.

E. Contribution of the polarization graph to the frequency mass

In the Hartree-Fock approximation, one has $\bar{m} = m$ and $m^* = \tilde{m}$. The nonvanishing contributions to the difference $\bar{m} - m$ therefore arise from the second-order polarization and correlation graphs and from higher order graphs. Limiting ourselves to second order, we write

$$\frac{\bar{m}(k)}{m} = \frac{\bar{m}_{PO}(k)}{m} + \frac{\bar{m}_{CO}(k)}{m} - 1, \tag{5.17}$$

with

$$\frac{\bar{m}_{PO}(k)}{m} = 1 - \left[\frac{\partial}{\partial \omega} V_{PO}(k; \omega) \right]_{\omega = e(k)}, \tag{5.18}$$

$$\frac{\bar{m}_{CO}(k)}{m} = 1 - \left[\frac{\partial}{\partial \omega} V_{CO}(k; \omega) \right]_{\omega = e(k)}. \tag{5.19}$$

In the present section we investigate the quantity $\bar{m}_{PO}$, i.e., the value that the frequency mass would

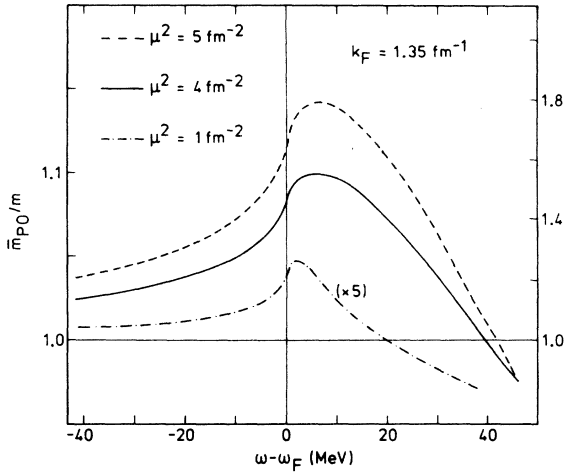

FIG. 6. Dependence upon the difference $\omega - \omega_F$ of the quantity $\bar{m}_{PO}/m$ defined in Eq. (5.20) for $k_F = 1.35$ fm^{-1} and $\mu^2 = 5$ fm^{-2} (dashes) 4 fm^{-2} (full curve) or 1 fm^{-2} (dash-and-dot curve). The left-hand scale corresponds to the strength $v_0/\mu^3 = 30$ MeV fm^3 and the right-hand scale to $v_0/\mu^3 = 70.6$ MeV fm^3.

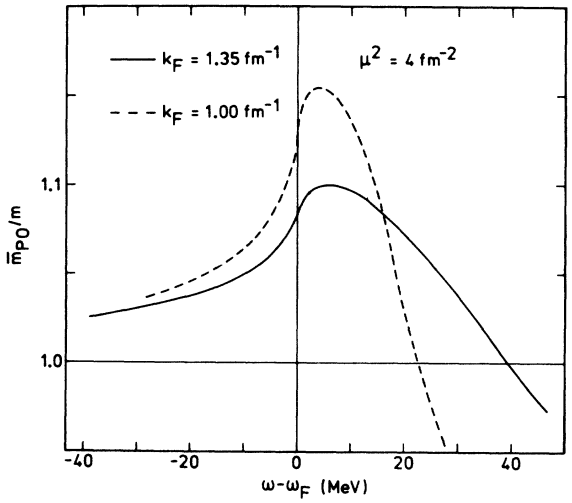

FIG. 7. Dependence upon $\omega - \omega_F$ of the quantity $\bar{m}_{PO}/m$ for $v_0/\mu^3 = 30$ MeV fm^3, $\mu^2 = 4$ fm^{-2}, and $k_F = 1.35$ fm^{-1} (full curve) or $k_F = 1.00$ fm^{-1} (dashed curve).

take if one only included the contribution of the second-order polarization graph. In keeping with Sec. V C, we maintain k fixed and equal to the Fermi momentum, and we calculate the quantity

$$\frac{\bar{m}_{PO}(\omega)}{m} = 1 - \frac{\partial}{\partial\omega} V_{PO}(k_F;\omega) \tag{5.20}$$

as a function of ω. This quantity can be obtained with great accuracy from the values of $V_{PO}(\omega)$ found in Sec. V C. The results are plotted versus the difference $\omega - \omega_F$ in Figs. 6 and 7, for various values of the parameters μ^2, v_0, and k_F.

We first discuss the striking feature that $\bar{m}_{PO}(\omega)$ presents an enhancement slightly above the Fermi surface.[11] Equation (5.11) implies that in the domain $\omega < \omega_F$ the quantity $\bar{m}_{PO}(\omega)$ is increasing with ω and is larger than m. At $\omega = \omega_F$, the logarithmic singularity (5.10) shows that $\bar{m}_{PO}(\omega)$ has an infinite positive slope since

$$\left[\frac{d}{d\omega}\frac{\bar{m}_{PO}(\omega)}{m}\right]_{\omega=\omega_F-0} = \frac{2}{(2\pi)^4}(\bar{m})^3\overline{|v|^2}\lim_{\omega\to\omega_F-0}\ln\left|\frac{\omega-\omega_F}{\omega_F}\right|. \tag{5.21}$$

From the dispersion relation (2.7) and from the asymptotic behavior (5.7) of $W_{PO}(k_F;\omega)$, one concludes that $\bar{m}_{PO}(\omega)$ has a maximum somewhat above ω_F and then decreases and becomes smaller than m. Although this behavior is in keeping with the value of $V_{PO}(\omega)$ shown in Fig. 5, we note that the latter do not exhibit any spectacular ω dependence near ω_F. This is why it is very difficult to obtain detailed information on the dependence of $\bar{m}_{PO}$ upon ω without an analytical model as we use here. Figure 7 shows that the enhancement peak becomes narrower when k_F decreases. In a local density approximation, this would correspond to the property that the enhancement of $\bar{m}_{PO}(\omega)$ is less pronounced at high density, i.e., in the nuclear interior, than at low density, i.e., at the nuclear surface. We emphasize, however, that here this is not related to the existence of surface vibrations, nor of a density-dependent interaction. The narrowing of the enhancement peak with decreasing k_F reflects the shift towards smaller values of ω of the location of the maximum of $W_{PO}(\omega)$.

We now turn to a comparison between our results and the perturbation approach of Ref. 11. There, the quantities $V_{PO}(k;\omega)$ and $\bar{m}_{PO}(k)$ [Eq. (5.18)] were estimated analytically for k close to k_F and ω close to ω_F, in the framework of a perturbation expansion in powers of the ratio $|k - k_F|/\mu$. We found significant differences between our results and those presented in Ref. 11. These originate from the fact that several inaccurate approximations were made in Ref. 11. In particular, it was assumed there as well as in Ref. 13 that the quantity p defined in Eq. (5.3) is close to k_F, and that furthermore some integrals over $|\vec{a} - \vec{b}|$ can be extended to infinity.

F. Momentum distribution

One of the interests of the decomposition (5.17) of the frequency mass is that the quantities $\bar{m}_{PO}(k)/m$ and $\bar{m}_{CO}(k)/m$ are directly related to

the momentum distribution in the correlated ground state, as we now briefly recall. In the uncorrelated ground state, the momentum distribution is given by $n_<(k)$ [Eq. (2.3)]; all momentum states k are fully occupied up to the Fermi momentum k_F and are empty for $k > k_F$. In the presence of correlations, nucleons can be excited above the Fermi surface. In second order, the momentum distribution in the correlated ground state is given by

$$\rho(k) = 2 - [m_{PO}(k)/m] \tag{5.22}$$

for $k < k_F$, and by

$$\rho(k) = [m_{CO}(k)/m] - 1 \tag{5.23}$$

for $k > k_F$. As above, we shall approximate the quantity $\bar{m}_{PO}(k)$ which is defined in Eq. (5.18) by the quantity $\bar{m}_{PO}[e(k)]$ defined in Eqs. (2.5) and (5.20). This is quite accurate but is exact only for $k = k_F$. The dependence of $\rho(k)$ upon the ratio k/k_F is represented in Fig. 8. The domain $k > k_F$ will be discussed in Sec. VI. As expected from Sec. V.E, cf. Figs. 6 and 7, $\rho(k)$ has a vertical slope at $k = k_F - 0$. This property holds for any normal Fermi system.[12] We note that it only emerges from approximation schemes which include *low-lying* excitations of the system. In particular, it did not appear in the standard version of the Brueckner-Hartree-Fock approximation in which these low-lying excitations were excluded. It also does not appear in most variational calculations,[27-34] because these use for the correlation function an expression which does not account for the existence of long-range correlations.

G. Comparison with realistic interactions

In the present section, we briefly compare the matrix elements (3.3) of the nucleon-nucleon interaction used in the present model with the matrix elements of Brueckner's reaction matrix g. In Fig. 9, we compare the diagonal element

$$\langle q|v|q\rangle = \frac{8\pi\mu v_0}{(\mu^2 + 2q^2)^2}, \tag{5.24}$$

where $\vec{q} = \frac{1}{2}(\vec{k} - \vec{j})$, with the diagonal elements $\langle q|g|q\rangle$ of the reaction matrix in the ^1S and ^3S channels, as calculated by Siemens[35] from Reid's soft core interaction and for $p = \frac{1}{2}|\vec{k} + \vec{j}| = 0.14$ fm^{-1}. We see that the parameter set (4.2a) yields fair agreement with the diagonal elements of the reaction matrix. This nice agreement unfortunately does not apply to the off-diagonal elements of the g matrix. This gives rise to the following problem. The depletion of the Fermi sea can be characterized by the quantity $\kappa = 1 - \rho(k_{av})$, where $k_{av} = 0.75\, k_F$ is the average momentum of a nucleon in the Fermi sea. The quantity κ is the "smallness parameter" which governs the rate of convergence of the Bethe-Brueckner hole line expansion for the binding energy of nuclear matter.[36] In the present model one has $\kappa = 0.035$ for the parameter set (4.2a) at the Fermi momentum $k_F = 1.35$ fm^{-1}. This value of κ is much smaller than the one obtained from the Brueckner-Hartree-Fock approximation with a realistic nucleon-nucleon interaction. For

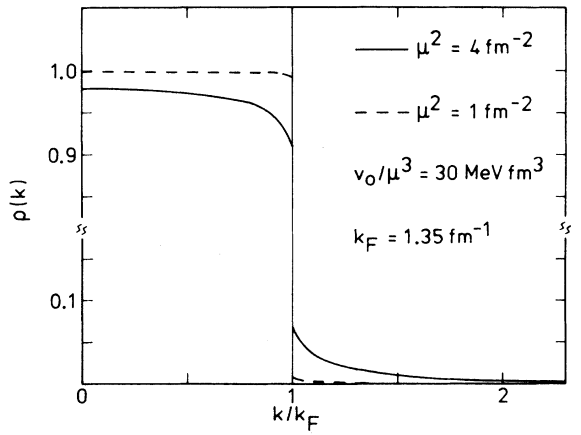

FIG. 8. Momentum distribution in the correlated ground state of nuclear matter for $v_0/\mu^3 = 30$ MeV fm^3, $k_F = 1.35$ fm^{-1}, and $\mu^2 = 4$ fm^{-2} (full curve) or $\mu^2 = 1$ fm^{-2} (dashed curve).

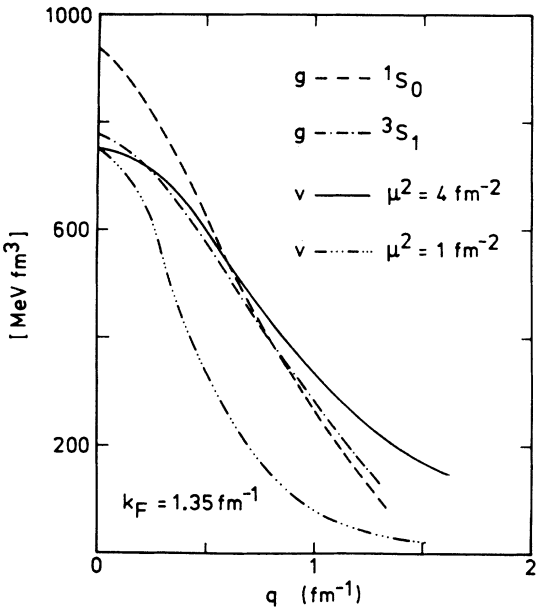

FIG. 9. The diagonal element (5.24) of the model interaction is represented by the full curve for $\mu^2 = 4$ fm^{-2}, $v_0/\mu^3 = 30$ MeV fm^3, and by the dash-and-three-dots curve for $\mu^2 = 1$ fm^{-2}, $v_0/\mu^3 = 30$ MeV fm^3. The diagonal elements of Brueckner's g matrix (Ref. 35) are represented by the full curve for the ^1S channel and by the dash-and-dot curve for the ^3S channel, for $k_F = 1.35$ fm^{-1}.

instance, Reid's hard core nucleon-nucleon interaction yields $\kappa \approx 0.25$.[11] Thus, our model does not appear to give a realistic value for κ, nor consequently for $\bar{m}_{PO}/m$, whenever the input parameters are adjusted in such a way that the first-order approximation to the self-energy is reasonably accurate. We now discuss the origin of this problem.

In our model the nucleon-nucleon interaction only acts in relative s-wave states. A more realistic model should take into account the existence of a tensor force which couples the $^3S_1$ and $^3D_1$ states. This tensor force yields the dominant contribution to κ. For instance, Table 6 of Ref. 37 indicates that this coupling accounts for approximately fifty percent of the value of κ. This suggests that it would be reasonable to renormalize our results for $(\bar{m}_{PO}/m) - 1$ by about a factor of 2. In the case $\mu^2 = 4$ fm^{-2} for instance, this renormalization would correspond to favoring a strength $v_0/\mu^3 \approx 50$ MeV fm^3 over the value $v_0/\mu^3 = 30$ MeV fm^3. Several questions arise in this connection. The first one consists in wondering whether it is not inconsistent to use different interaction strengths for the first order graph on the one hand and for the second order graphs on the other hand. We believe that this is not necessarily so. Indeed, the tensor part of the effective interaction does not contribute to the Hartree term and only yields a small contribution to the Fock (exchange) term. Hence, the first order graph is not very sensitive to the omission of the tensor interaction, in contradistinction to the value of κ. A more serious problem concerns the validity of trying to make the model more realistic by simply readjusting the strength v_0/μ^3 so as to make the corresponding value of κ coincide with that calculated from a realistic nucleon-nucleon interaction. This appears quite dubious. Indeed, the range of the tensor force in momentum space is larger than that of the central force. Hence, the tensor force is able to excite high-lying intermediate states, very much like a hard core interaction. This would be likely to add a smooth background to $\bar{m}_{PO}/m$, rather than to contribute to the enhancement peak proper. This is discussed below.

H. Dependence upon core excitation energies

The imaginary part of the optical-model potential at the energy ω' differs from zero because of the existence of open decay channels. In the present framework, the analogous statement is that $W_{PO}(\omega')$ differs from zero because of the existence of one-particle–one-hole core excited states with excitation energy smaller than $\omega' - \omega_F$. Hence, one way of studying the effect upon $\bar{m}_{PO}(\omega)$ of low-lying core excited states consists in setting a cutoff energy ω_M in the dispersion integral which appears in Eq. (2.7). We thus assume that the quantity

$$V_{PO}^{M}(\omega) = \frac{P}{\pi} \int_{\omega_F}^{\omega_F + \omega_M} \frac{W_{PO}(\omega')}{\omega - \omega'} d\omega' \tag{5.25}$$

corresponds to the value that the real part of the polarization graph would take if one would not include in the calculation any core state with excitation energy larger than ω_M. The dependence of $V_{PO}^{M}(\omega)$ upon ω_M is of practical interest for the following reason: When calculating the polarization graph in finite nuclei one is forced to truncate the configuration space. A question thus arises concerning the importance of the omitted core excitations. Hamamoto and Siemens[10] find that core states at several tens MeV excitation energy still yield a sizable contribution to V_{PO} and to $\bar{m}_{PO}$. While we agree with this finding, we now show that these high-lying states only provide a smooth background to $\bar{m}_{PO}/m$ in the vicinity of the Fermi surface.

The quantity

$$\frac{\bar{m}_{PO}^{M}(\omega)}{m} = 1 - \frac{\partial}{\partial \omega} V_{PO}^{M}(\omega) \tag{5.26}$$

is represented in Fig. 10 for the cutoff energies

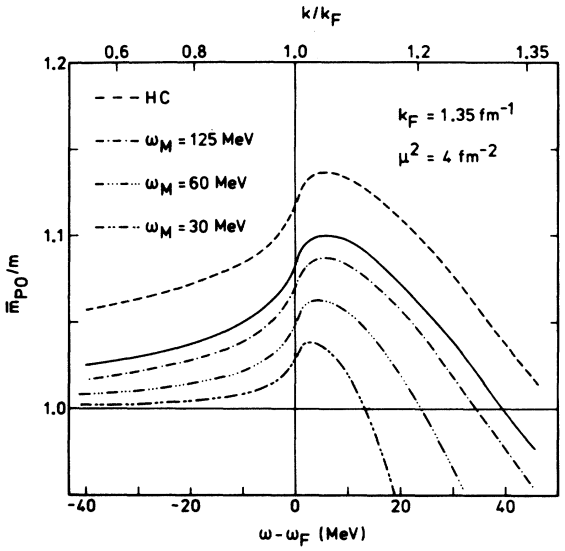

FIG. 10. The full curve represents the value of $\bar{m}_{PO}(\omega)/m$, as calculated from our model for $k_F = 1.35$ fm^{-1}, $\mu^2 = 4$ fm^{-2}, and $v_0/\mu^3 = 30$ MeV fm^3. The value of $\bar{m}_{PO}^{M}(\omega)/m$ [Eq. (5.26)] is represented by the dash-and-dot line ($\omega_M = 125$ MeV), the dash-and-three-dots curve ($\omega_M = 60$ MeV), and the dash-and-two-dots curve ($\omega_M = 30$ MeV). The dashed line corresponds to the model modified in order to simulate the effect of a hard core; see Eq. (5.28).

$\omega_M = 30$, 60, and 125 MeV. The great similarity between the curves demonstrates that high-lying core excited states indeed only give rise to a smooth background to $\bar{m}_{PO}(\omega)$, and essentially do not contribute to the enhancement peak proper. These results make one expect that, conversely, the effect of a short range repulsion would essentially amount to adding a smooth background to the value of $\bar{m}_{PO}(\omega)/m$ calculated from our model. This is what we now confirm.

A hard core repulsion mainly influences the excitation of high-lying core states, and accordingly the value of $W_{PO}(\omega)$ at high energy. This is illustrated by the differerence between the asymptotic behavior (5.6) which holds in our model and the asymptotic behavior (5.7) of W_{PO}^{HS} which corresponds to the hard sphere Fermi gas model. In order to simulate the effect of a hard core, let us add to $W_{PO}(\omega)$ for large ω a function which has the same asymptotic behavior as $W_{PO}^{HS}(\omega)$. More explicitly, let us retain the value of $W_{PO}(\omega)$ given by our model up to the frequency ω_q for which $W_{PO}(\omega_q)$ is maximum. In the example $\mu^2 = 4$ fm^{-2}, $k_F = 1.35$ fm^{-1}, one has $\omega_q - \omega_F = 125$ MeV. For $\omega > \omega_q$, let us add to $W_{PO}(\omega)$ the following function $W_{PO}^{HS}(\omega)$, chosen in such a way that its derivative vanishes at $\omega = \omega_q$ and that it has the asymptotic behavior (5.7):

$$W_{PO}^{HS}(\omega) = \frac{2}{\pi}(k_F c)^2 \frac{k_F}{\tilde{m}^{1/2}} (\omega^{1/2} + \omega_q^{3/2}/2\omega - \tfrac{3}{2}\omega_q^{1/2})\theta(\omega - \omega_q). \quad (5.27)$$

The only additional parameter contained in this modified model is the hard sphere radius c. Let us take $c = 0.52$ fm as in Ref. 12. In the modified model, the imaginary part of the polarization graph is given by

$$W_{PO}^{HC} = W_{PO}(\omega) + W_{PO}^{HS}(\omega); \quad (5.28)$$

it is represented by the dashed curve in the upper part of Fig. 5. The corresponding real part of the polarization graph as calculated from the subtracted dispersion relation (5.8) is represented by the dashed curve in the lower part of Fig. 5. The associated frequency mass is represented by the dashed curves in Fig. 11. There the component $W_{PO}(\omega)$ has been computed for $\mu^2 = 4$ fm^{-2}, with a strength $v_0/\mu^3 = 56$ MeV fm^3 chosen in such a way that $\kappa^{HC} \approx 0.25$. We note that this modified model is in very good agreement with the value of $\bar{m}_{PO}(\omega)/m$ calculated from the Brueckner-Hartree-Fock approximation with Reid's hard core interaction. In contradistinction, our unmodified model would yield too high and too narrow an enhancement peak if one simply renormalized the strength to the value $v_0/\mu^3 = 77$ MeV fm^3 which corresponds to

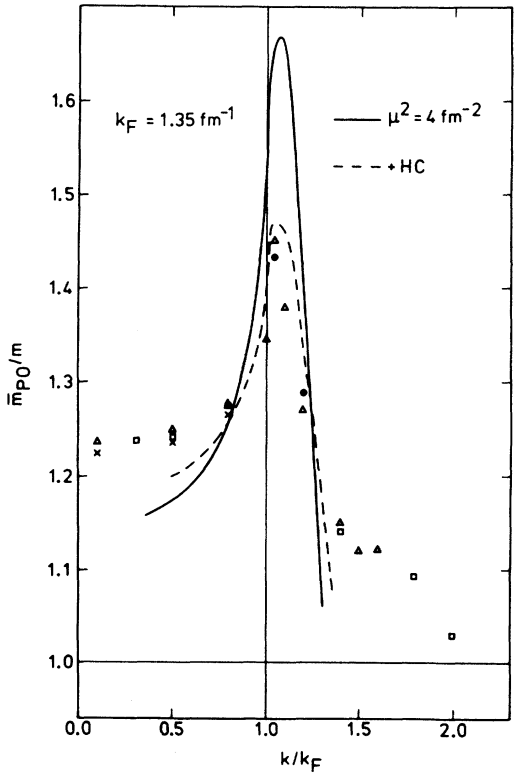

FIG. 11. The triangles, dots, and squares are taken from Ref. 11. They represent values of $\bar{m}_{PO}/m$ calculated from the Brueckner-Hartree-Fock approximation with Reid's hard core nucleon-nucleon interaction, for $k_F = 1.35$ fm^{-1}. The full line corresponds to the present model, with $v_0/\mu^3 = 77$ MeV fm^3 and $\mu^2 = 4$ fm^{-2}. The dashed curve takes into account the effect of a hard core as indicated by Eq. (5.28) with $v_0/\mu^3 = 56$ MeV fm^3, $\mu^2 = 4$ fm^{-2}.

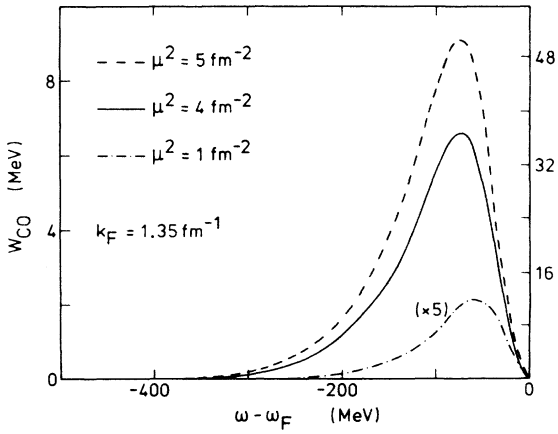

FIG. 12. Dependence upon the difference $\omega - \omega_F$ of the imaginary part of the correlation graph for $k_F = 1.35$ fm^{-1} and for $\mu^2 = 1$ fm^{-2} (dash-and-dot curve), $\mu^2 = 4$ fm^{-2} (full curve), or $\mu^2 = 5$ fm^{-2} (dashes). The left-hand scale corresponds to the potential strength $v_0/\mu^3 = 30$ MeV fm^3 and the right-hand scale to $v_0/\mu^3 = 70.6$ MeV fm^3.

$\kappa \approx 0.25$. This is illustrated by the full curve in Fig. 11. Similar results hold for $k_F = 1.10$ fm^{-1}.

VI. CONTRIBUTION OF THE CORRELATION GRAPH

A. Introduction

One of the main interests of the present study is that we are able to calculate accurately the contribution of the correlation graph to the frequency mass. This had previously only been achieved in the case of the dilute hard sphere Fermi gas model.[12] Let us first paraphrase the discussion of the polarization graph in Sec. V A. The second order polarization contribution to the single-particle field is represented by the graph labeled (CO) in Fig. 1. For $k > k_F$ its physical interpretation is the following: When a nucleon with momentum $k > k_F$ is added to the correlated ground state of nuclear matter, the Pauli principle blocks the admixture in this correlated ground state of those two-particle–two-hole configurations in which one of the particles has momentum k; whence the expression "correlation graph." In the case $k < k_F$, the physical interpretation of this graph is the following [see Eq. (2.6)]: If a hole with momentum k and frequency ω is punched into the ground state of nuclear matter, it can excite a two-hole $(\vec{j},\vec{l})$, one-particle $(\vec{a})$ configuration. This is a real excitation if energy is conserved, i.e., if $\omega = e(j) + e(l) - e(a)$; otherwise it is a virtual excitation. The real excitations give rise to an imaginary component of the mean field, namely

$$W_{CO}(k;\omega) = \frac{\pi}{2}\sum_{\vec{j},\vec{l},\vec{a}} n_<(j) n_<(l) n_>(a) \times |\langle \vec{j},\vec{l}|v|\vec{k},\vec{a}-\vec{a},\vec{k}\rangle|^2 \times \delta(\omega + e(a) - e(j) - e(l)) . \quad (6.1)$$

The real part of the correlation graph reads

$$V_{CO}(\omega) = \tfrac{1}{2}\sum_{\vec{j},\vec{l},\vec{a}} n_<(j) n_<(l) n_>(a) \times \frac{|\langle \vec{j},\vec{l}|v|\vec{k},\vec{a}-\vec{a},\vec{k}\rangle|^2}{\omega + e(j) - e(a) - e(b)} , \quad (6.2)$$

where the summation sign implies a principal value integral whenever the energy denominator on the right-hand side vanishes. Momentum conservation requires that

$$\vec{j} + \vec{l} = \vec{k} + \vec{a} (= 2\vec{p}) . \quad (6.3)$$

As in the case of the polarization graph, it is advantageous to first calculate the imaginary part

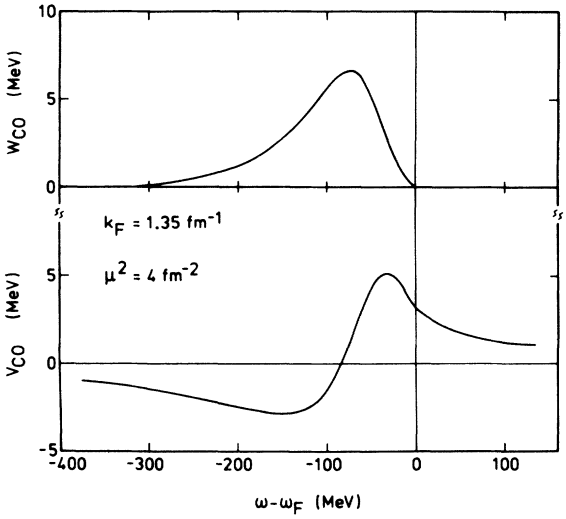

FIG. 13. Dependence upon $\omega - \omega_F$ of the quantities $W_{CO}(\omega)$ (upper part) and $V_{CO}(\omega)$ (lower part) in the case $\mu^2 = 4$ fm^{-2}, $k_F = 1.35$ fm^{-1}, and $v_0/\mu^3 = 30$ MeV fm^3.

$W_{CO}(\omega) = W_{CO}(k_F;\omega)$ of the correlation graph, and to subsequently calculate the real part $V_{CO}(\omega) = V_{CO}(k_F;\omega)$ from the dispersion relation (2.8). We shall use the effective mass approximation $e(q) = q^2/2\tilde{m}$.

B. Imaginary part of the correlation graph

The algebraic expression of $W_{CO}(\omega)$ is too lengthy to be given here; it is available upon request. The dependence of $W_{CO}(\omega)$ upon the difference $\omega - \omega_F$ is shown in Fig. 12. These results can be compared with those shown in Fig. 4 for $W_{PO}(\omega)$. One sees that $W_{CO}(\omega)$ is practically equal to $W_{PO}(\omega)$ for $|\omega - \omega_F| < 60$ MeV. This is due to the fact that the asymptotic behavior of $W_{CO}(\omega)$ for ω close to ω_F is also given by Eq. (5.5). For large values of $|\omega - \omega_F|$, however, $W_{CO}(\omega)$ decreases faster than $W_{PO}(\omega)$; this is a general feature. Indeed, the asymptotic value of $W_{PO}(\omega)$ is given by Eq. (5.6); this corresponds to a smooth decrease with increasing $\omega - \omega_F$. In contradistinction, $W_{CO}(\omega)$ identically vanishes for $\omega - \omega_F < -8\omega_F$ as a consequence of energy and momentum conservation.[12] We can conclude from this discussion that $W_{CO}(\omega)$ has a peak which is narrower than that of $W_{PO}(\omega)$, with a maximum which occurs at a somewhat smaller value of $|\omega - \omega_F|$.

C. Real part of the correlation graph

The dispersion relation (2.8) shows that $V_{CO}(\omega)$ is positive and has a negative slope for ω larger than ω_F; by continuity this remains true for ω

somewhat smaller than ω_F. Hence, $V_{CO}(\omega)$ and $V_{PO}(\omega)$ have opposite signs for ω close to ω_F. However, their derivatives have the same sign. The fact that $W_{PO}(\omega)$ is in general larger than $W_{CO}(\omega)$ entails that $|V_{PO}(\omega_F)| > |V_{CO}(\omega_F)|$. We note incidentally the erroneous character of one claim made in Ref. 9, where it was stated that $V_{PO}(\omega_F)$ is equal to $-V_{CO}(\omega_F)$ for an infinite Fermi gas. The shape of $W_{CO}(\omega)$ and the dispersion relation (2.8) imply that $V_{CO}(\omega)$ has a typical dispersive wiggle below the Fermi surface. This is displayed in Fig. 13.

D. Contribution of the correlation graph to the frequency mass

We now discuss the quantity

$$\frac{\bar{m}_{CO}(\omega)}{m} = 1 - \frac{\partial}{\partial\omega} V_{CO}(\omega) \tag{6.4}$$

which represents the value that the frequency mass takes when only the correlation graph is included. The discussion can follow that of $\bar{m}_{PO}$ in Sec. V. The quantity $\bar{m}_{CO}(\omega)$ has an infinite negative slope at $\omega = \omega_F$. From the shape of $V_{CO}(\omega)$ shown in Fig. 13, one concludes that $\bar{m}_{CO}(\omega)$ has a maximum for ω somewhat smaller than ω_F. This is exhibited in Figs. 14 and 15. The comparison of these figures with Figs. 6 and 7 shows that at a semiquantitative level $\bar{m}_{CO}(\omega)$ and $\bar{m}_{PO}(\omega)$ are almost symmetric of one another with respect to ω_F.

Equation (5.23) shows that the momentum distribution above the Fermi surface is given by

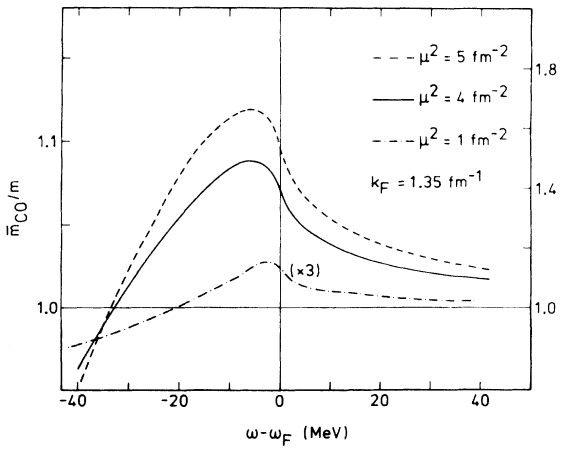

FIG. 14. Dependence upon the difference $\omega - \omega_F$ of the quantity $\bar{m}_{CO}/m$ defined in Eq. (6.4) for $k_F = 1.35$ fm^{-1} and $\mu^2 = 5$ fm^{-2} (dashes), 4 fm^{-2} (full curve), or 1 fm^{-2} (dash-and-dot curve). The left-hand scale corresponds to the strength $v_0/\mu^3 = 30$ MeV fm^3 and the right-hand scale to $v_0/\mu^3 = 70.6$ MeV fm^3.

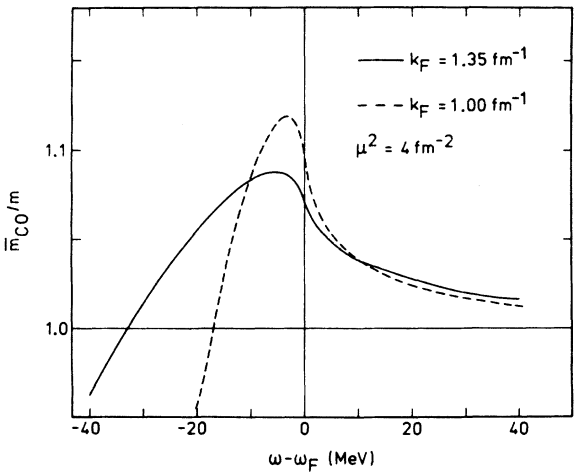

FIG. 15. Dependence upon $\omega - \omega_F$ of the quantity $\bar{m}_{CO}/m$ for $\mu^2 = 4$ fm^{-2}, $v_0/\mu^3 = 30$ MeV fm^3, and $k_F = 1.35$ fm^{-1} (full curve) or $k_F = 1.00$ fm^{-1} (dashed curve).

$$\rho(k) \approx \frac{\bar{m}[e(k)]}{m} - 1\,, \tag{6.5}$$

where the sign $\approx$ corresponds to our approximation of keeping k fixed and equal to k_F when computing $\bar{m}_{CO}(\omega)$. The curves shown in Figs. 9 and 10 for $k > k_F$ have been calculated from Eq. (6.5). The sum rule

$$3k_F^{-3}\int_0^\infty \rho(k)k^2\,dk = 1 \tag{6.6}$$

is exactly fulfilled when $\bar{m}_{PO}(k)$ and $\bar{m}_{CO}(k)$ are calculated from Eqs. (5.22) and (5.23). A measure of the error introduced by setting $k = k_F$ when calculating $\bar{m}_{CO}(\omega)$ and $\bar{m}_{PO}(\omega)$ therefore consists in checking to what extent the sum rule (6.6) is violated. In the case $\mu^2 = 4$ fm^{-2}, $k_F = 1.35$ fm^{-1} for instance, the full curve shown in Fig. 8 yields the value 1.066 for the left-hand side of Eq. (6.6). We conclude that our approximation for calculating $\bar{m}_{CO}(\omega)$ is fairly accurate, especially in the domain $0.5\,k_F < k < 1.5\,k_F$ in which we are mainly interested in the present context.

By proceding in the same way as in Sec. V H we can study the dependence of $\bar{m}_{CO}(\omega)$ upon the size of the configuration space by introducing cutoff energies in the dispersion relation (2.8). We thus define the quantity

$$V_{CO}^{M}(\omega) = \frac{P}{\pi}\int_{\omega_M+\omega_F}^{\omega_F} \frac{W_{CO}(\omega')}{\omega - \omega'}\,d\omega'\,. \tag{6.7}$$

It can be identified with the value that the correlation graph would take if one would include all one hole excited states with excitation energy larger than ω_M. The associated quantity

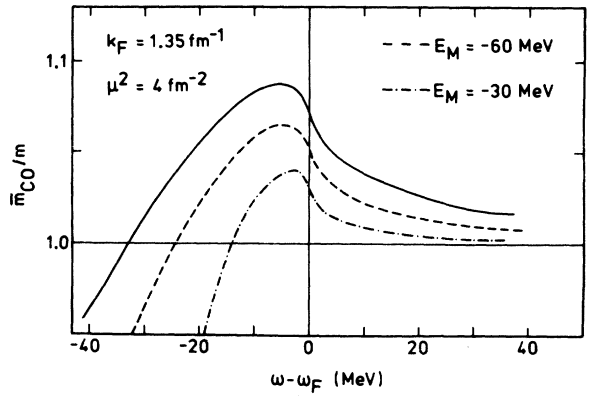

FIG. 16. The full curve represents the value of $\bar{m}_{CO}/m$ as calculated from our model for $k_F = 1.35$ fm^{-1}, $\mu^2 = 4$ fm^{-2}, and $v_0/\mu^3 = 30$ MeV fm^3. The value of $\bar{m}^M_{CO}(\omega)/m$ [Eq. (6.8)] is represented by the dashed curve for $\omega_M = -60$ MeV and by the dash-and-dot line for $\omega_M = -30$ MeV.

$$\frac{\bar{m}^M_{CO}(\omega)}{m} = 1 - \frac{\partial}{\partial \omega} V^M_{CO}(\omega) \tag{6.8}$$

is represented in Fig. 16. We see that the high-energy excitations essentially contribute to a smooth background the value of $\bar{m}_{CO}(\omega)$. The enhancement peak is thus due to low-lying excitations, as was also the case for the quantity

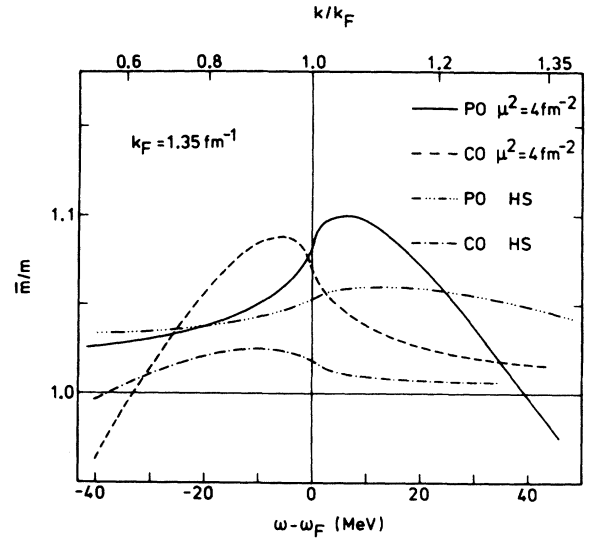

FIG. 17. The full and the dashed curves represent the values of $\bar{m}_{PO}(\omega)/m$ and $\bar{m}_{CO}(\omega)/m$, respectively, as calculated from the present model with $k_F = 1.35$ fm^{-1}, $\mu^2 = 4$ fm^{-2}, and $v_0/\mu^3 = 30$ MeV fm^3. The dash-and-three-dots curve and the dash-and-dot line represent the values of $\bar{m}_{PO}(\omega)/m$ and of $\bar{m}_{CO}(\omega)/m$, respectively, as calculated from the dilute hard sphere Fermi gas model.[12] They are normalized so as to correspond to the same value of the depletion κ as the present model.

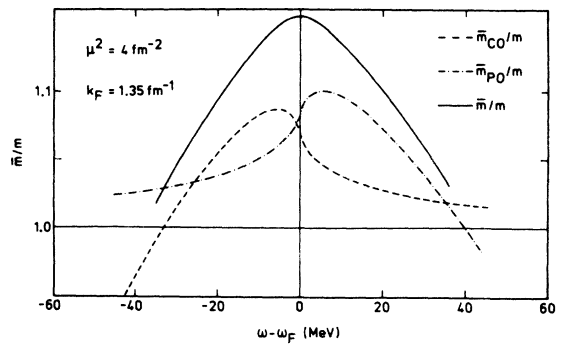

FIG. 18. Dependence upon the difference $\omega - \omega_F$ of the quantities $\bar{m}_{PO}/m$ (dash-and-dot curve), $\bar{m}_{CO}/m$ (dashes), and $\bar{m}/m$ (full curve), in the case $\mu^2 = 4$ fm^{-2}, $k_F = 1.35$ fm^{-1}, and $v_0/\mu^3 = 30$ MeV fm^3.

$\bar{m}_{PO}(\omega)$. In the hard sphere Fermi gas model, all intermediate states have the same coupling to the single-particle states, since in that model the matrix elements $\langle \vec{k}, \vec{j} | v | \vec{a}, \vec{b} \rangle$ are replaced by a constant. In that model, low-lying excitations are therefore not preferentially excited and we expect a weaker enhancement of $\bar{m}_{PO}(\omega)$ and of $\bar{m}_{CO}(\omega)$ near the Fermi energy. This is exhibited in Fig. 17.

VII. THE EFFECTIVE MASS

A. The frequency mass

The second-order approximation to the frequency mass $\bar{m}$ is written in Eq. (5.17) as the sum of the

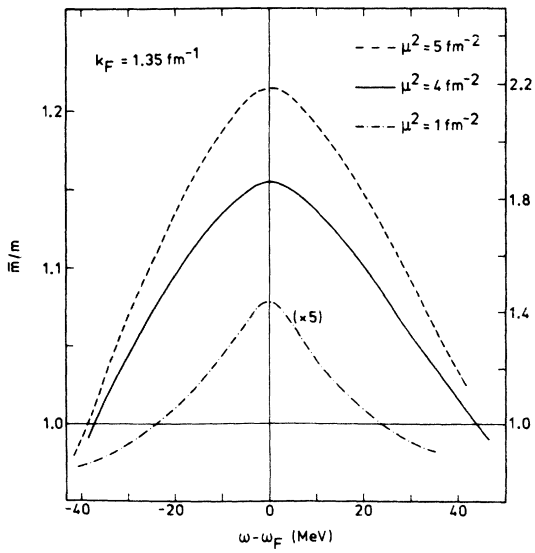

FIG. 19. Dependence of the quantity $\bar{m}/m$ upon the difference $\omega - \omega_F$ for $k_F = 1.35$ fm^{-1}, and $\mu^2 = 5$ fm^{-2} (dashes), $\mu^2 = 4$ fm^{-2} (full curve), or $\mu^2 = 1$ fm^{-2} (dash-and-dot curve). The left-hand scale corresponds to $v_0/\mu^3 = 30$ MeV fm^3 and the right-hand scale to $v_0/\mu^3 = 70.6$ MeV fm^3.

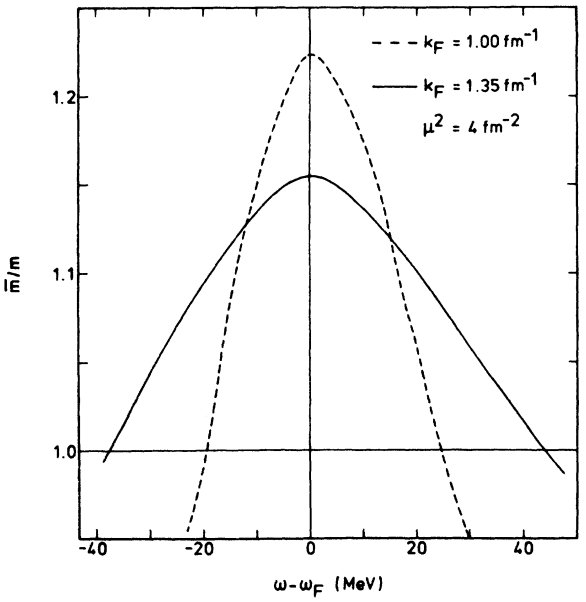

FIG. 20. Dependence of the quantity $\bar{m}/m$ upon $\omega-\omega_F$ for $\mu^2=4$ fm^{-2}, $v_0/\mu^3=30$ MeV fm^3, and $k_F=1.00$ fm^{-1} (dashes) or $k_F=1.35$ fm^{-1} (full curve).

two skew-symmetric quantities $\bar{m}_{PO}(\omega)$ and $\bar{m}_{CO}(\omega)$. Figures 18–20 show that the enhancement peak of $\bar{m}$ is practically symmetric about $\omega=\omega_F$. It is therefore possible to define rather unambiguously the width Γ of this enhancement peak. The parameters of our model are v_0, μ, and k_F. When $\bar{m}/m$ is plotted versus k/k_F, the width Γ is independent of v_0, which only determines the ordinate scale. Since k_F sets the momentum scale, the width Γ is a well-defined function of the ratio μ/k_F of the momentum range to the Fermi momentum. Figure 21 shows that Γ decreases when μ decreases, for fixed k_F. It also decreases when k_F increases. One must, however, keep in mind that Γ is the width of the enhancement peak of the function $\bar{m}/m$ when this quantity is plotted versus k/k_F. The width Δ of the function $\bar{m}/m$ when plotted versus the energy ω, as in Figs. 19 and 20, is given by

$$\Delta \approx 2\,\omega_F \Gamma\,. \tag{7.1}$$

When k_F decreases for fixed μ, Γ increases less rapidly than $\omega_F \approx k_F^2/2\tilde{m}$ decreases. Consequently, Δ rapidly decreases when k_F decreases. This is exhibited in Fig. 20. For instance, one has $\Delta \approx 48$ MeV for $k_F=1.35$ fm^{-1}, and $\Delta \approx 28$ MeV for $k_F=1.00$ fm^{-1}, in the case $\mu^2=4$ fm^{-2}.

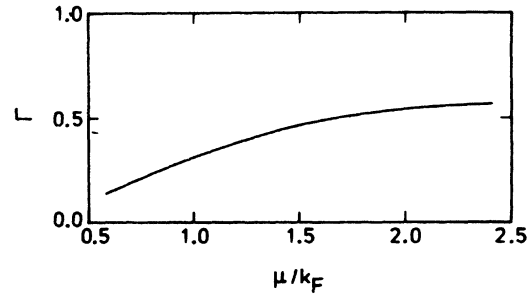

FIG. 21. Dependence upon μ/k_F of the width Γ of the enhancement peak that $\bar{m}/m$ displays when it is plotted versus k/k_F.

B. The effective mass

Equation (5.14) states that the full effective mass m^* is the product of $\bar{m}/m$ by the momentum mass $\tilde{m}$. The quantity m^*/m is plotted versus k/k_F in Fig. 22, in the case $\mu^2=4$ fm^{-2}, $k_F=1.35$ fm^{-1}, and $v_0/\mu^3=30$ MeV fm^3. As we discussed in Sec. V G, our model underestimates the background value of $\bar{m}/m$. In order to correct for this deficiency, let us tentatively multiply $\tilde{m}$ by a modified $\bar{m}/m$ calculated as follows. We take $\bar{m}_{PO}(\omega)/m$ from the dashed curve in Fig. 13. This corresponds to the inclusion of a hard sphere tail to $W_{PO}(\omega)$ and to the parameter values $\mu^2=4$ fm^{-2}, $v_0/\mu^3=56$ MeV fm^3. The latter value of v_0/μ^3 is now adopted for calculating the modified $\bar{m}_{CO}/m$. The resulting m^*/m is represented in Figs. 23 and 24. While we admit that this is the result of ap-

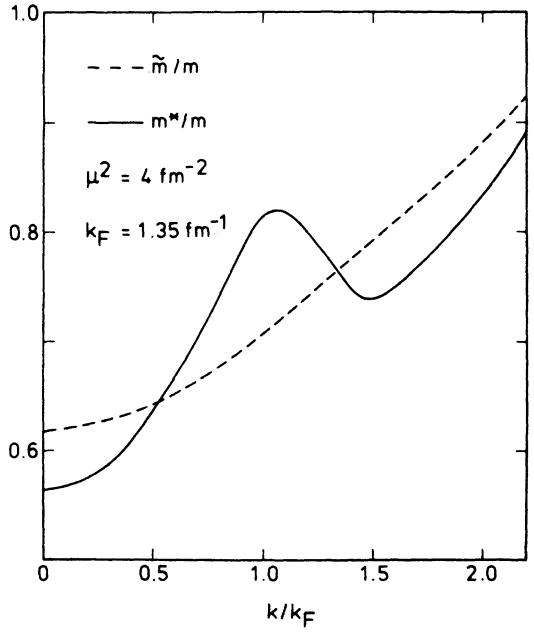

FIG. 22. Dependence upon k/k_F of the quantities $\tilde{m}/m$ (dashed curve) and m^*/m (full curve), as calculated at $k_F=1.35$ fm^{-1} for $\mu^2=4$ fm^{-2} and $v_0/\mu^3=30$ MeV fm^3.

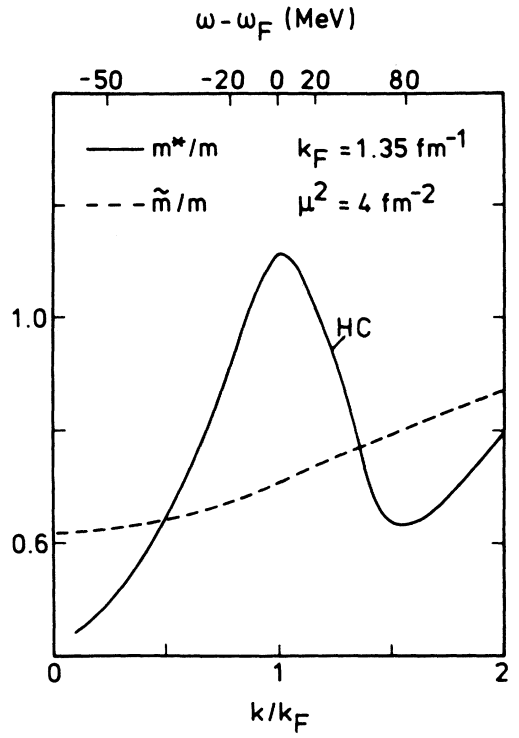

FIG. 23. The dashed line represents $\tilde{m}/m$ for $\mu^2=4$ fm^{-2}, $k_F=1.35$ fm^{-1}, and $v_0/\mu^3=30$ MeV fm^3. The full curve corresponds to the value of m^*/m that is obtained by multiplying $\tilde{m}/m$ by an effective mass $\bar{m}$ which includes semiquantitatively the effect of a tensor interaction and of a short-range repulsion, as described at the end of Sec. VII B.

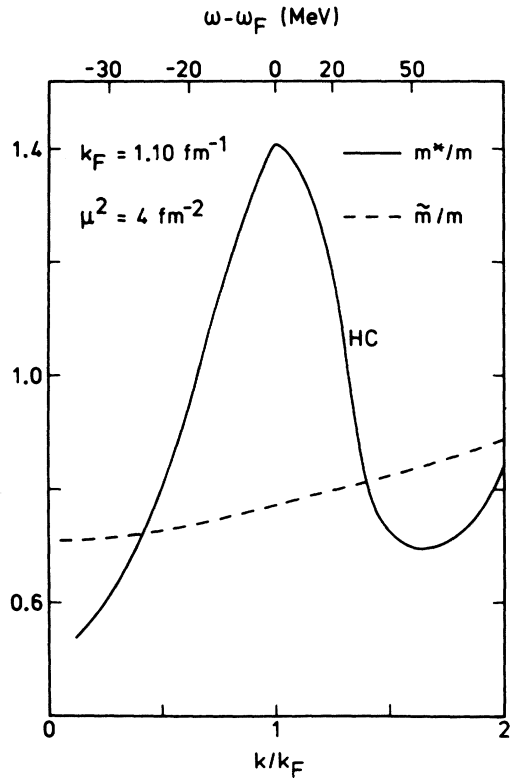

FIG. 24. Same as Fig. 23 for $k_F=1.10$ fm^{-1}.

proximate manipulations, we believe that Figs. 23 and 24 give semiquantitative information on the behavior of the effective mass in the realistic case, for $k_F=1.35$ fm^{-1} and $k_F=1.10$ fm^{-1}, respectively. We note that the enhancement peak is much more pronounced and is narrower at low than at high density.

VIII. SUMMARY

In the present paper, we investigated in detail the frequency dependence of the self-energy of nuclear matter near the Fermi energy. The self-energy is calculated up to second order in the strength of the nucleon-nucleon interaction. We used a simple parametrization for the matrix elements of the nucleon-nucleon interaction. We saw in Secs. IV and V G that our parametrization of the diagonal matrix elements is fairly realistic; the corresponding Hartree-Fock field is thus satisfactory. The off-diagonal elements of our interaction are less realistic mainly because we do not include the effect of a tensor interaction and of a hard core repulsion. We showed in Secs. V G, V H, and VI D that these omitted features would only yield a smooth background contribution to most of the quantities of interest, in particular to the effective mass. Hence, our model can be considered as semirealistic. Moreover, we described in Sec. V G that the model can be modified so as to yield very good agreement with the frequency dependence of the polarization graph as calculated from the Brueckner-Hartree-Fock calculation with a realistic nucleon-nucleon interaction. We have been able to calculate the correlation graph and its contribution to the effective mass and to the momentum distribution. This had previously been possible only for the much more academic case of the dilute hard sphere Fermi gas model. This represents a significant improvement since the role of the correlation graph turns out to be as important as that of the polarization graph. We confirmed and investigated in detail the fact that the contribution of the polarization graph to the effective mass has a narrow and skew peak which reaches its maximum somewhat above the Fermi surface. We showed that the contribution of the correlation graph to the effective mass also has a narrow and skew peak, which in this case reaches its maximum somewhat below the Fermi

surface. We demonstrated that these features are quite independent of the detailed nature of the interaction. When plotted as a function of the quasiparticle energy, the sum of the polarization and correlation contributions yields a peak which is nearly symmetric about the Fermi energy. We note that this is at variance with the parametrization adopted in Ref. 5 where only the polarization graph was taken into account. The width of the enhancement peak decreases with decreasing nuclear density. It also decreases when the range of the effective nucleon-nucleon interaction increases. The latter property reflects the dominant role played by the low-lying excitations in the enhancement of the effective mass near the Fermi surface. This was illustrated in Secs. V H and VID, where we showed that highly excited intermediate states only provide a smooth positive background to the effective mass. Qualitatively, we thus expect that in the case of finite nuclei the enhancement of the single-particle level density near the Fermi surface will be more pronounced and more localized because of the existence of low-lying collective states which are strongly coupled to single-particle levels.[2]

We are greatly indebted to G. E. Brown, A. K. Kerman, and B. Mottelson for having raised stimulating questions which prompted the present investigation. Useful discussions with Nguyen Van Giai are also gratefully acknowledged.

[1]B. Castel and K. Goeke, Phys. Lett. 82B, 160 (1979).
[2]G. E. Brown, J. S. Dehesa, and J. Speth, Nucl. Phys. A330, 290 (1979).
[3]G. E. Brown, Invited talk, Giant Multipole Resonance Topical Conference, Oak Ridge, Tennessee, 1979 (unpublished).
[4]A. Lejeune and C. Mahaux, *Proceedings of the 77th Enrico Fermi School, 1979* (North-Holland, Amsterdam, 1981).
[5]A. LeJeune, Nucl. Phys. A339, 317 (1980).
[6]V. Bernard and Nguyen Van Giai, *Proceedings of the 77th Enrico Fermi School, 1979* (North-Holland, Amsterdam, 1981).
[7]G. E. Brown, J. H. Gunn, and P. Gould, Nucl. Phys. 46, 598 (1963).
[8]P. Quentin and H. Flocard, Annu. Rev. Nucl. Sci. 28, 523 (1978).
[9]G. F. Bertsch and T. T. S. Kuo, Nucl. Phys. A112, 204 (1968).
[10]I. Hamamoto and P. Siemens, Nucl. Phys. A269, 199 (1976).
[11]J. P. Jeukenne, A. Lejeune, and C. Mahaux, Phys. Rep. 25C, 83 (1976).
[12]R. Sartor and C. Mahaux, Phys. Rev. C 21, 1546 (1980).
[13]K. A. Brueckner, Phys. Rev. 103, 172 (1956).
[14]K. A. Brueckner and D. T. Goldman, Phys. Rev. 117, 207 (1960).
[15]K. A. Brueckner, J. L. Gammel, and J. T. Kubis, Phys. Rev. 118, 1438 (1960).
[16]H. S. Köhler, Phys. Rev. 137, B1145 (1965).
[17]R. Sartor, Nucl. Phys. A267, 29 (1976).
[18]R. Sartor, Nucl. Phys. A289, 329 (1977).
[19]H. A. Bethe, Phys. Rev. 103, 1353 (1956).
[20]S. A. Moszkowski and B. L. Scott, Ann. Phys. (N.Y.) 11, 65 (1960).
[21]P. E. Hodgson, *Nuclear Reactions and Nuclear Structure* (Clarendon, Oxford, 1971).
[22]G. F. Bertsch, J. Borysowicz, H. McManus, and W. G. Love, Nucl. Phys. A284, 399 (1977).
[23]G. E. Brown, *Many-Body Problems* (North-Holland, Amsterdam, 1972).
[24]A. B. Migdal, Nucl. Phys. 30, 239 (1962).
[25]D. J. Thouless, Rep. Prog. Phys. 27, 53 (1964).
[26]R. S. Poggioli and A. D. Jackson, Phys. Rev. Lett. 35, 1211 (1975).
[27]P. M. Lam, J. W. Clark, and M. L. Ristig, Phys. Rev. B 16, 222 (1977).
[28]J. W. Clark, P. M. Lam, J. G. Zabolitsky, and M. L. Ristig, Phys. Rev. B 17, 1147 (1978).
[29]S. Fantoni, Nuovo Cimento 44A, 191 (1978).
[30]M. L. Ristig, P. M. Lam, and A. Lejeune, Phys. Lett. 93B, 240 (1980).
[31]S. Rosati, in *Proceedings of the Workshop on Meson Theory of Nuclear Forces and Nuclear Matter, Bad Honnef, 1979*, edited by D. Schütte, K. Holinde, and K. Bleuler (Bibliographisches Institut AG, Mannheim, Germany, 1980).
[32]A. Fabrocini, S. Fantoni, and A. Polls, private communication.
[33]O. Bohigas and S. Stringari, Phys. Lett. 95B, 9 (1980).
[34]M. L. Ristig and P. M. Lam, J. Low Temp. Phys. (in press).
[35]P. J. Siemens, Nucl. Phys. A141, 225 (1970).
[36]B. D. Day, Rev. Mod. Phys. 50, 495 (1978).
[37]A. Kallio and B. D. Day, Nucl. Phys. A124, 177 (1969).